Seismic performance of pile-supported bridge abutment resting on a liquefiable soil layer

Partha Saha & Akihiro Takahashi
Tokyo Institute of Technology, Meguro, Tokyo, Japan

ABSTRACT
A large-scale shake table test performed in Public Works Research Institute, Japan is numerically simulated by soil/water-coupled finite element analysis. 3D Finite Element Analysis (FEA) is conducted on two model abutments designed based on old and current Japanese standards for highway bridges. Abutments of a river crossing bridge are modeled. The abutments are supported by pile foundation and rest on the liquefiable soil layer. The numerical simulation can capture the overall response of the model abutment and surrounding soil. Both the experimental and numerical results confirm that accumulation of the displacement of the model ground and structural elements starts with the build-up of the excess pore water pressure. The abutment experiences backward rotation when there is a constraint in horizontal movement due to strut effect of the bridge girder in the model designed based on the old standard. This results in the difference in the bending moment profile. Observations in the experiments and numerical simulations are used to propose possible seismic retrofit of the piled abutments designed based on the old standard.

1 INTRODUCTION

The design consideration of an abutment of a river-crossing bridge is the most crucial issue while it is subjected to liquefaction-induced lateral spreading. Several simplified procedures are currently used to determine the kinematic demand due to lateral spreading. Because of a lot of uncertainties involved in lateral spreading phenomena, the simplified procedures cannot predict the dynamic response of the abutment properly. Moreover, the plain strain consideration in 2D analysis cannot incorporate the effect of the geometry of approach embankment which sometimes yields an excessively conservative design.

A clear demonstration of structural damages of the pile due to liquefaction during the 1964 Alaskan earthquake (Bartlett & Youd 1992) and again more recently during the 1995 Kobe earthquakes emphasized a design of resilient pile against lateral spreading. Thus, the design and construction of any megastructure like bridges in this kind of problematic soils (liquefiable soils) receive the attention of researchers. Regardless of a considerable number of experimental and numerical efforts (Motamed et al. 2013, and Takahashi et al. 2010) to understand the seismic response of pile or group of piles, the dynamic response of pile-supported bridge abutment in liquefied soil has rarely been studied.

Three-dimensional FE analysis was not convenient because of its high computational demand. However, it is gradually becoming popular with the development of the efficient computation system. Three-dimensional FE analysis is advantageous over any simplified procedures even the plain strain 2D analysis, as it incorporates the precise depiction of the size and the geometry of the model ground and its effect. Besides, the response of individual element at a different stage of loading can be precisely monitored in the 3D analysis.

A three-dimensional finite element analysis is carried out to simulate a large-scale shake table test performed in Public Works Research Institute (PWRI). Both the experiment and the numerical simulation are conducted on model abutment designed based on current Japanese standard for highway bridges (Japan Road Association 2002). Ground motion data of Tohoku Earthquake, 2011 is applied to examine the effect of longer duration earthquake. The response of the bridge abutment designed based on the old Japanese standard (Japan Road Association 1964) under Kobe Earthquake and the effect of the geometry of the approach embankment are also studied.

2 OVERVIEW OF THE EXPERIMENTAL PROGRAM

Bridge abutments including the approach embankments are designed and modelled with a scale of 1:10 in these experiments. Two different configurations of model abutments are incorporated in these experiments. In Experiment-1, the model abutment is designed according to the current Japanese design standards for highway bridges and in Experiment-2 & 3, the model abutments are designed based on the old Japanese design standards. The detail description of both model abutments is given in the next section. A 6 m × 3 m × 2 m steel container is used to prepare the model ground. The base of the container is fixed to the shaking table. In order to examine the effect of the shape of the embankment, two different configurations of the approach embankment are made. In Experiment-1 & 2 the widths of the embankment are kept 3.0 m which are equal to the width of the model container whereas, in Experiment-3, a limited extent of the embankment is considered. In Experiment-3, the top width of the approach embankment is equal to the width of the abutment having a side slope of 1:2 both in transverse and longitudinal directions. The plan and cross-sectional views of the experimental setups are shown in Figure 1 to Figure 3. A lifted water tank is used to saturate the foundation soil and the flow of the water from the base of the container is continued until constant head of water is reached in the standpipe.

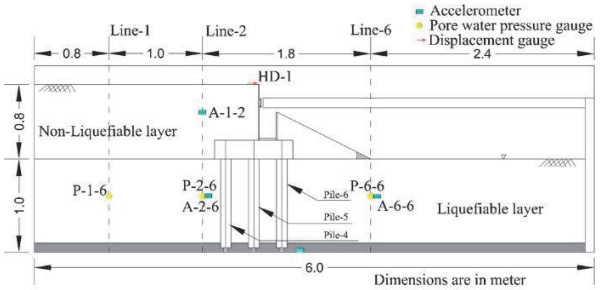

Figure 1: Longitudinal section of the experimental setup of Experiment-1.

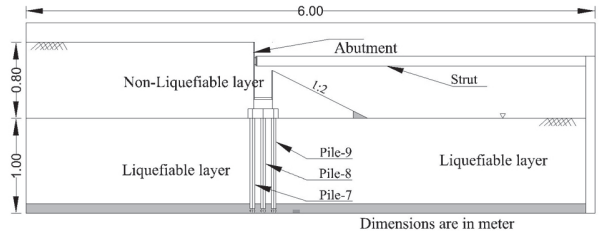

Figure 2: Longitudinal section of the experimental setup of Experiments-2 & 3.

2.1 Description of the model abutment

The model abutment in Experiment-1 is supported by a 3 × 4 pile group. The piles are hinged at its tip to the container to prevent the translational movement of the pile group. The head of the piles is rigidly attached to the footing of the abutment. The half width of the bridge abutment is modeled to take advantage of symmetry. Because of that reason only six piles are visible in the plan view. The piles are designed with a 1.10 m long steel (SS400) bar having a cross-sectional dimension of 31 mm × 25 mm in order to adjust to the bending stiffness of the pile design based on the current design standard. In fact, the old standard allows the closely spaced flexible piles whereas, the current standard recommends using comparatively stiff piles with wider spacing. A series of a circular ring having an outer diameter of 114.3 mm are attached to the pile along its length to impose the effect of the volume of the piles. The longitudinal section and the plan view of the experimental setup are shown Figure 1 and Figure 3(a) respectively.

A strut, rigidly fastened to the experiment container, is placed in front of the abutment to simulate the strut effect of the bridge girder. Current Japanese design standard for highway bridges recommends using a comparatively large gap between the face of the abutment to the edge of the bridge girder. The gap between the strut and the abutment in Experiment-1 is kept 20 mm to avoid the frequent collision. The physical properties of the piles are summarized in Table 1.

The model is subjected to Tohoku Earthquake ground motion applied with an appropriate similitude law (Muir Wood 2004). Similarly, two other experiments are conducted to examine the response of the bridge abutment designed based on the old Japanese standard. Based on the old Japanese standard, the abutment is supported by 3 × 8 pile group. The physical properties of the pile are described in Table 2. In Experiment-3, the width of the embankment is limited to the equal width of the abutment and in Experiments-1 & 2 the width is considered to be semi-infinite. To observe the strut effect of the bridge girder the gap between the strut and bridge abutment in Experiments-2 & 3 is kept smaller which is only 5 mm.

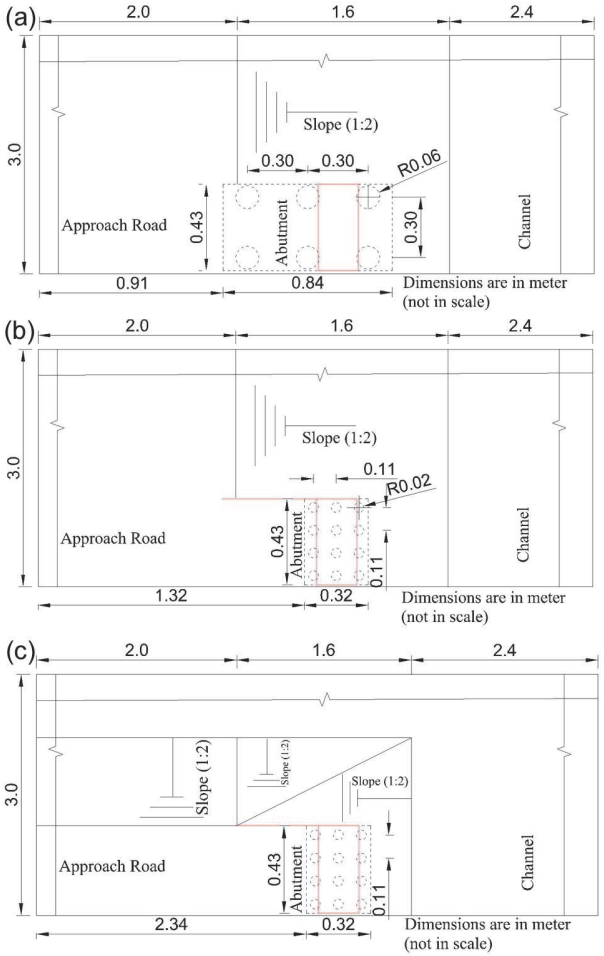

Figure 3: Plan view of experimental setup of (a) Experiment-1, (b) Experiment-2, and (c) Experiment-3.

2.2 Preparation of the model ground

As it is mentioned earlier, the model ground is built inside a large container having the dimensions of 6 m × 3 m × 2 m in length, width, and height respectively. Silica Sand No. 6 with a relative density of 50% is used to make the embankment as well as the foundation soil which are placed over a drainage layer with a thickness of 100 mm. The dry deposition method is used to prepare the model ground and then compacted by tamping to reach up to the desired level of compaction. The foundation soil up to the base of the pile cap is kept saturated to ensure liquefaction of that soil during shaking. The physical properties of Silica Sand No. 6 are listed in Table 3.

Table 1: Physical properties of Piles in Experiment-1.

Element type	Properties
Pile upholding (each pile)	
Dimensions (mm)	1105×31×25
Modulus of elasticity (N/m^2)	2×10^{11}
Mass (kg)	6.72
Circular ring (each pile)	
Outer diameter (mm)	114.3
Inner diameter (mm)	112.3
Height (mm)	810
Material type	Steel (SUS304)
Mass (kg)	4.50

Table 2: Physical properties of piles in Experiments-2 & 3

Element type	Properties
Pile upholding (each pile)	
Dimensions (mm)	1102×19×8
Modulus of elasticity (N/m^2)	2×10^{11}
Mass (kg)	1.31
Circular ring (each pile)	
Outer diameter (mm)	48.6
Inner diameter (mm)	46.6
Height (mm)	864
Material type	Steel (SUS304)
Mass (kg)	2.0

Table 3: Physical properties of Silica Sand No. 6.

Physical properties	Silica Sand No. 6
Specific gravity, G_s	2.647
Relative density, D_r (%)	50
Dry density (g/cm^3)	1.467
Maximum dry density (g/cm^3)	1.314
Minimum dry density (g/cm^3)	1.661
Uniformity coefficient, U_c	2.08
Void ratio, e_0	0.804
Maximum void ratio, e_{max}	1.014
Minimum void ratio, e_{min}	0.594
Permeability (m/s)	5.15×10^{-4}

3 THREE-DIMENSIONAL FINITE ELEMENT ANALYSIS

In this study, a finite element code developed by Takahashi (2002) is used to simulate the shake table test results described in the previous section. A fully coupled u-p formulation is used in this finite element code. The governing equation of an infinitesimal soil element considering the moment balance relation of the solid-fluid matrix can be expressed as Eq. 1.

$$L^T \sigma - \rho \ddot{u} + \rho b = 0 \qquad [1]$$

Where $\ddot{u}$ represents the acceleration of the solid matrix, $\rho = [(1-n)\ \rho_s + n\ \rho_f]$ is the total density, n is the porosity of the porous material, ρ_s is the density of the solid particle, ρ_f is the density of the water, and b is the body force, σ is the stress tensor representing the total stress, and L is the differential operator. Combining the flow conservation equation, moment balance of fluid and generalized Darcy's seepage law, the governing equation for pore fluid can be written as Eq. 2.

$$\frac{k}{\rho_f g}\nabla^T(\nabla p + \rho_f b) + m^T \dot{\varepsilon} - \frac{n\dot{p}}{K_f} = 0 \qquad [2]$$

Where k is the hydraulic conductivity, ∇ is a differential operator, p is the pore pressure, ε is the strain, $m = [1\ 1\ 1\ 0\ 0\ 0]^T$ for three-dimensional cases, n is the porosity, and K_f is the bulk moduli of pore fluid. Eq.1 and Eq. 2 together with the constitutive equations define the behavior of porous solid and pore water pressure.

3.1 Finite element model

The finite element meshes used in these numerical analyses for Experiment-1, Experiment-2, and Experiment-3 are designated with Model-1, Model-2, and Model-3 respectively as shown in Figure 4. The soil materials, the footing, and the stem of the abutment are modeled as 8-nodes brick elements whereas, the piles are modeled as elastic beam elements. The whole domain is divided into a number of uniform meshes except near the structural elements, where comparatively finer meshes are used to arrange the structural members. The 0.2 m × 0.2 m × 0.2 m brick elements are used to model most of the domain of the liquefiable layer and the 0.2 m × 0.2 m × 0.1 m brick elements are used in the case of non-liquefiable approach embankment. Smaller brick elements for approach embankment are used to accommodate the 1:2 slope of the embankment.

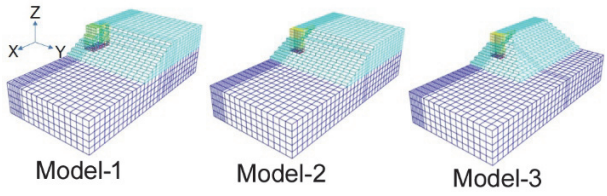

Figure 4. Finite element meshes for Model-1, Model-2, and Model-3.

3.2 Boundary conditions

The boundary conditions are selected in such a way that it can resemble the experimental conditions. Any kind movement of the nodes at the bottom boundaries of the domain is restricted. All the nodes along the vertical boundary wall are constrained to move normal towards

the vertical wall, however, they are set free to move vertically and in the directions parallel to the vertical walls. All other nodes inside the domain of the analysis are set free to move in any direction. The fluid flow velocities perpendicular to the boundaries of the analytical domain are set to zero. In order to simulate the "strut effect" of the bridge girder in Models-2 & 3, the horizontal movement near the top of the abutment, where the strut and the abutment wall colloid during shaking is constrained. However, the abutment is free to move in the vertical direction. One limitation of this assumption is that in reality, the abutment walls in Models-2 & 3 are capable of moving backward having a limited forward movement but in the numerical model, both the backward and the forward movement is restricted. It is believed that, although there exists a continuous accumulation of displacement in the forward direction, the effect of this simplification will be minimized.

3.3 Material parameters

The soil elements are modeled as an elastoplastic material and a constitutive model proposed by Asaoka et al. (2002) is used to predict the cyclic behavior of sand. This model is an advanced constitutive model that can consider the decay of internal structure of the soils. The difference between clay and sand can be distinguished by considering super-loading surfaces together with rotational hardening in modified cam-clay model. Seventeen parameters are required to formulate the soil model out of which κ and λ are the tangent of the swelling and the virgin compression line and can be determined from consolidation test. e_0, v, and G_s are the initial void ratio, Poisson's ratio and specific gravity of the soil which can be determined from element tests. All other parameters are determined by trial and error so that the numerical liquefaction resistance curve closely fits the experimental one. Soil parameters are listed in Table 4.

The typical stress path, stress-strain curve, and the comparison of experimental numerical liquefaction resistance curve using the above-mentioned soil parameters under cyclic loading are presented in Figure 5, and Figure 6 respectively. Again, the abutment and the piles are modeled as an elastic solid elements and beam elements respectively. In reality, the piles sometimes go under significant rotation due to the development plastic hinge. However, the objective of this study is to examine the location of the peak bending moment and its magnitude. Therefore, the consideration of the piles as an elastic element does not have a significant effect on the overall response of the abutment. The parameters are summarized in Table 5.

3.4 Input ground motion

Acceleration time history recorded by an accelerometer which is attached to the base of the container during the experiment is used in this analysis as an input ground motion. The recorded data may contain background noise from different sources. Most of the noises are non-seismic and remain in the range of low or high frequency (Kramer 1996). This kind of high-frequency or low-frequency acceleration data which is beyond the engineering interest needs to be isolated from the recorded data. Another correction is also introduced to avoid the permanent displacement at the end of motion is commonly known as baseline correction. A computer based software (Seismosignal-2016) is used for baseline correction and to obtain a bandpass filtered (frequencies in between 0.1 Hz to 25 Hz) ground motion data. The input ground motion for Model-1 (Experiment-1) is shown in Figure 7.

Table 4: Soil parameters for numerical analysis.

Parameters	Liquefiable layer	Crustal layer
κ	0.004	0.004
λ	0.05	0.05
G_s	2.65	2.65
e_0	0.804	0.804
v	0.33	0.33
φ	35	35
φ_d	38	38
b_r	3.0	3.0
m	0.1	0.1
a	2.7	2.7
R	1.0	1.0
R_0*	0.25	0.25
K_0	0.5	0.5
k (m/sec)	5.14×10^{-04}	5.14×10^{-04}

Table 5: Material parameters for structural elements.

Element type	Parameters	Experiment-1	Experiment-2 & 3
Vertical wall	ρ (Mg/m^3)	1.02	1.59
	E	2.10×10^{11}	2.10×10^{11}
	v	0.26	0.26
Footing	ρ (Mg/m^3)	0.29	2.10
	E	2.10×10^{11}	2.10×10^{11}
	v	0.26	0.26
Pile	EI (N-m^2)	8.46×10^{3}	1.70×10^{3}
	EA	1.62×10^{8}	31.92×10^{6}

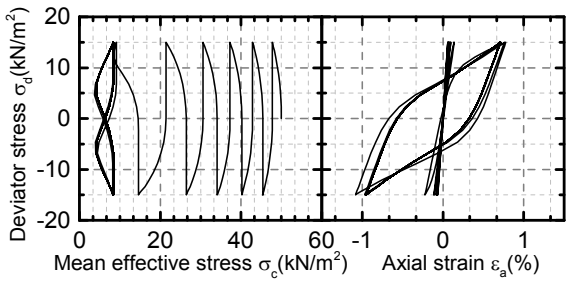

Figure 5: Typical stress path and stress-strain curve under cyclic loading.

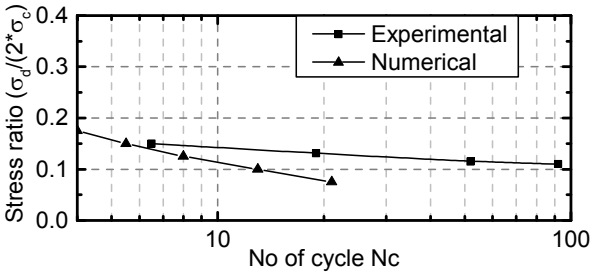

Figure 6: Comparison of numerical and experimental liquefaction resistance curve.

Since the three-dimensional FEA requires a long time for computation, therefore, the ground motion data of a comparatively short duration earthquake is also used in the case of Models–2 & 3 as well as Model-1 to observe the strut effect and the effect of the shape of the embankment. Considering the catastrophe of the Kobe Earthquake the ground acceleration data of Kobe Earthquake is used in his analysis which is shown in Figure 8.

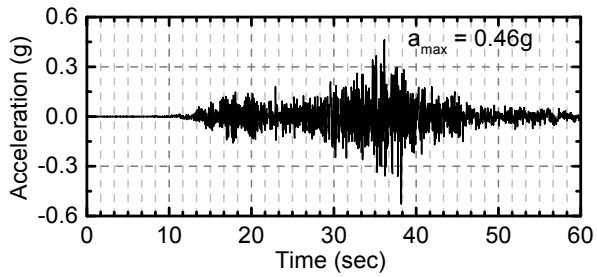

Figure 7: Input ground motion for Model-1 (Tohoku Earthquake)

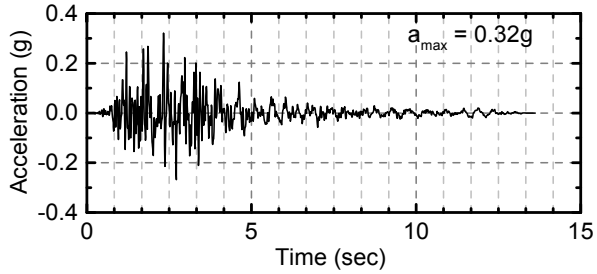

Figure 8: Input ground motion (Kobe Earthquake).

4 COMPARISON OF NUMERICAL AND EXPERIMENTAL RESULTS.

The obtained ground response in numerical analysis is much more severe than it is observed in the experiment. The model ground in numerical analysis is subjected to a significant lateral spreading and goes under a large surface settlement. The deformed shape, and horizontal displacement (*x*-direction) and vertical settlement (*z*-direction) at the shoulder (point “S” marked in Figure 9) of the embankment are depicted in Figure 9 and Figure 10 respectively.

Figure 10 shows a considerably large horizontal displacement of the embankment which reaches nearly about 300 mm, while the maximum horizontal displacement was 20 mm in Experiment-1. It signifies the displacement is approximately 3.0 m in real scale. Although this is apparently large, but this kind of excessive lateral spreading was observed in the past earthquakes. For example, during 1990 Luzon earthquake in Philippines, the right bank of Pantal river near Magsaysay Bridge which was underlain by sand deposits, was subjected to a liquefaction-induced lateral flow of about 5.0 m (Amiri 2008).

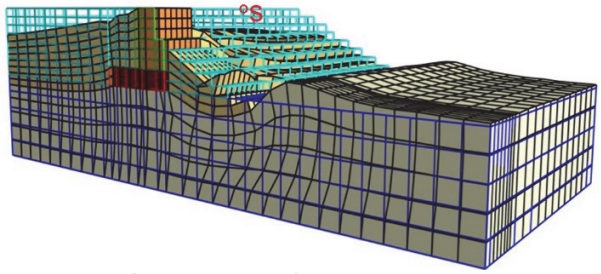

Figure 9: Deformed shape of the model ground.

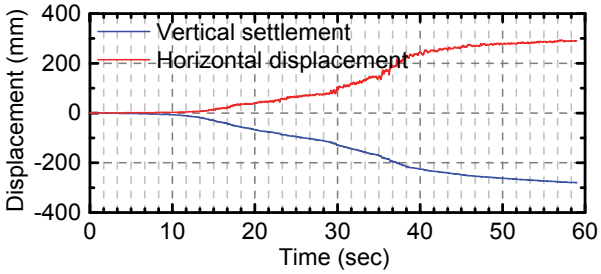

Figure 10: Horizontal displacement and vertical settlement of point "S" marked in Figure 9.

4.1 Generation of pore water pressure

A comparison of computed and experimental results of pore water pressure at three different locations underneath the embankment and inside the channel are shown in Figure 12. The numerical results represented by red lines in the illustration show a quick development of pore water pressure. Almost all the cases, there is a sharp increase in pore water pressure after 10 secs of shaking whereas, in experimental results, the generation of major pore water pressure starts after 30 secs of shaking. Besides, the magnitude of pore water pressure especially underneath the embankment is considerably large in comparison with the experimental results. Inside the channel, the magnitude of the maximum computed pore water pressure is almost equal to the experimental values.

The distribution of computed pore pressure ratio, which is expressed as the pore water pressure divided by the initial effective stress, throughout the model ground is

illustrated in Figure 11. While the pore pressure ratio reaches to the unit value, the corresponding soil mass is considered to be liquefied. According to the illustration, almost all parts of the foundation soil both underneath the embankment and inside the channel get liquefied. It is evident from Figure 11 and Figure 12 that the experimental pore water pressure underneath the embankment was not large enough to make the soil liquefied. However, the foundation soil inside the channel gets liquefied during the experiment as well as in numerical analysis.

The degree of saturation of the model ground plays an important role in the occurrence of liquefaction. Usually, the liquefaction resistance of soil is significantly increased with the decrease in the degree of saturation. In fact, the cyclic behavior of the partially saturated sand resembles the behavior of a densely saturated sand (Yoshimi et al. 1989) that requires a large number of cycles to reach to liquefaction. It implies that the rate of pore water pressure generation is also significantly affected by the degree of saturation. Probably the relatively low degree of saturation in the experiments is the main cause of this kind of inconsistency between the experimental and numerical results of pore water pressure generation.

4.2 Ground response

A comparison of computed and experimental acceleration time histories at three different points, which are inside the backfill, inside the liquefiable layer underneath the embankment, and inside the channel are shown in Figure 13. Although the computed acceleration time history inside the backfill cannot perfectly capture the peaks of the experimental results, but the computed results are quite comparable. However, a significant de-amplification in the magnitude of acceleration is observed inside the liquefiable layer. This phenomenon is frequently observed in the liquefied soil during a real earthquake. Because of the substantial loss of shear strength during liquefaction, the soils lose its capacity to transfer shear wave and consequently the de-amplification of the acceleration time histories takes place.

4.3 Horizontal displacement of the abutment

Figure 14 illustrates the computed and measured horizontal displacement at the crest of the abutment. The computed results indicated by red line show a significant contrast with experimental results. The computed lateral movement is excessively larger than it is observed in the experiment. During lateral spreading, while the foundation soil gets liquefied, the upper crustal layer moves towards the channel and it pushes the structures. Since the foundation soil in numerical analysis completely gets liquefied, the abutment is subjected to a comparatively large earth pressure due to the movement of the backfill which causes an excessively large horizontal movement of the abutment.

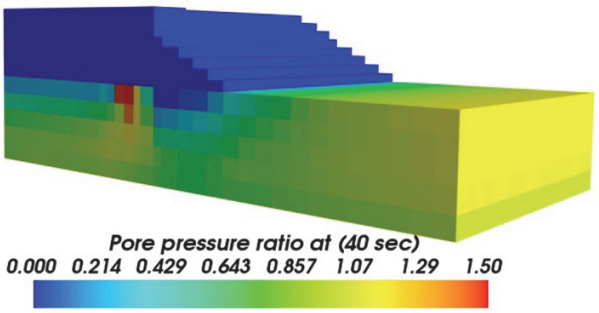

Figure 11: Distribution of pore pressure ratio throughout the model ground.

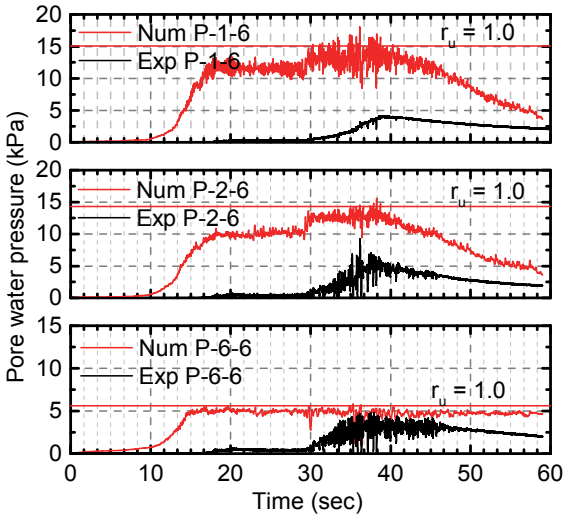

Figure 12: Comparison of computed and experimental pore water pressure.

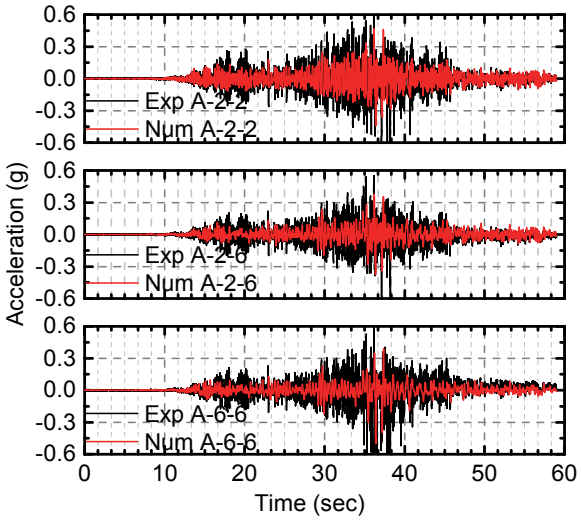

Figure 13: Comparison of computed and experimental acceleration time histories.

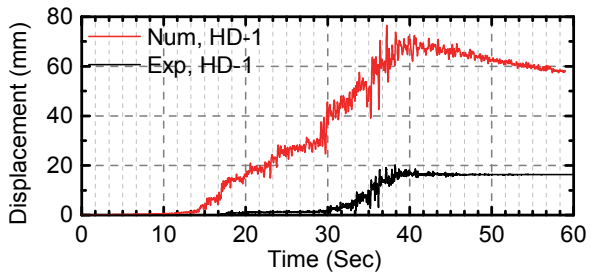

Figure 14: Comparison of the horizontal movement of the abutment.

Besides, the abutment shows a tendency of backward movement after 40 secs and finally reaches to a permanent displacement of approximately 60 mm. It is to be mentioned here, that the time history shows an early generation of pore water pressure which triggers the movement of the soil and structural elements earlier in numerical analysis. The tendency of backward movement of the abutment is probably caused due to the significant loss of shear strength of the foundation soil. During liquefaction, the soils lose its capacity to prevent the backward movement of the stiff piles, eventually, the abutment tends to rebound to its original position.

4.4 Bending moment of pile

A comparison of computed and experimental bending moment profiles for Pile-4, Pile-5, and Pile-6 while the pile heads are experiencing maximum bending moment are shown in Figure 15. The red color solid lines represent the computed bending moment isochrone, whereas, the black dots denote the measured bending moments in the experiment. It is evident that the maximum bending moment both in the experiment and numerical analysis took place near the head of the piles. Although the distributions are similar, the maximum computed bending moment is significantly large in comparison with the experimental values. The response of a pile supported abutment in liquefied soil is directed by a complex interaction between the piles and the surrounding soil which is influenced by several factors, for example, the amount of relative displacement of the crustal layer, the stiffness of the piles and so forth. Because of the severe liquefaction of the foundation soil, the horizontal movement of the crustal layer far from the structure in the transverse direction is considerably large. Which implies that the crustal layer imposes huge passive pressure to the comparatively stiff pile supported abutment and consequently, the piles are subjected to a large bending moment.

The computed bending moment distribution patterns of all the piles, Pile-4, Pile-5, and Pile-6, are almost similar. Another important thing is that the critical bending moment is unlikely to coincide with the principal shocks of the input ground motion. Therefore, the direct consideration of the inertia force of the backfill soil mass due to principal shocks may not provide the true critical bending moment due to lateral spreading.

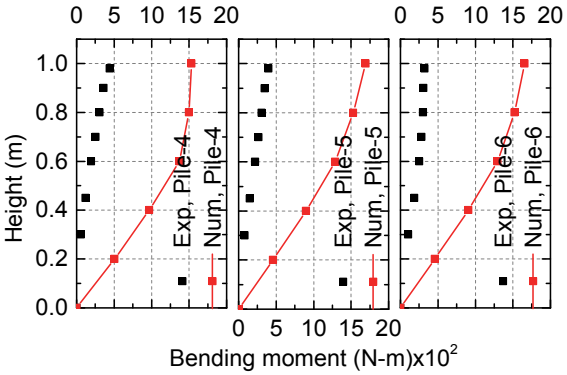

Figure 15: Computed and experimental bending moment profile at Pile-4, Pile-5, and Pile-6.

5 STRUT EFFECT OF THE BRIDGE GIRDER

In Experiments-2 & 3, a rigidly fastened strut is placed extremely close (only 5 mm) to the face of the abutment to examine the strut effect of the bridge girder. In the experiment, the model abutment is designed based on the old Japanese standard for highway bridge design. Numerically, the effect of the strut is modeled by imposing a constraint on the horizontal movement of the abutment. In order to complete the analysis faster, the Kobe Earthquake ground motion data as shown in Figure 8 is used as an input ground motion. In order to compare the dynamic response of the abutment, both the Model-1 and Model-2 are analyzed. The comparison of maximum bending moment distribution of piles in Model-1 and Model-2 under Kobe ground motion data is shown in Figure 16.

The strut effect completely changes the bending moment distribution profile. The red color line represents the bending moment profile for Model-2 where there is a constraint in horizontal movement of the abutment. Two different peaks are observed, one exists at the middle height of the pile and the another one is near the pile head. A similar response is also observed in experimental results. This kind of bending moment distribution implies a backward rotation of the abutment. In these circumstances, a significant part of the horizontal forces imposed due to lateral spreading is shared by the strut causing a considerable reduction of bending moments along the piles.

6 EFFECT OF THE WIDTH OF EMBANKMENT

The abutment is subjected to the destabilizing forces from the soil mass inside the probable wedge of failure and the side frictions caused due to the flow of side soils. In order to examine the effect of the width of the embankment in failure mechanism, an abutment model similar to the Model-2 with a finite width of the embankment at its top, which is regarded as Model-3, is analyzed. The response of the model abutment is also studied under Kobe Earthquake motion. The comparison of the maximum bending moment is illustrated in Figure 17. The figure

represents that all the piles in Model-3 are experiencing a smaller bending moment in comparison with the piles in Model-2. Although the percentage of reduction of bending moment are varying with the position of the pile but quantitatively almost 25 percent of the maximum bending moment is reduced due to the removal of the extended part of the embankment.

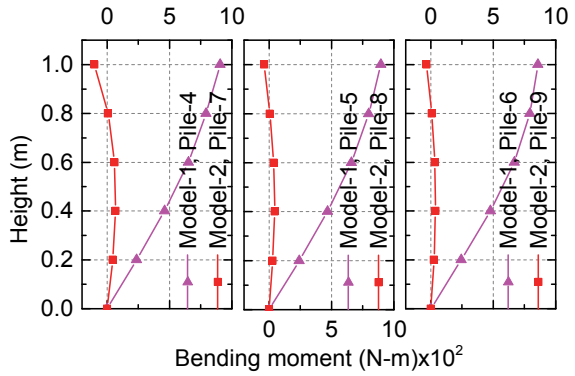

Figure 16: Maximum bending moment distribution of piles in Model-1 and Model-2 under Kobe Earthquake.

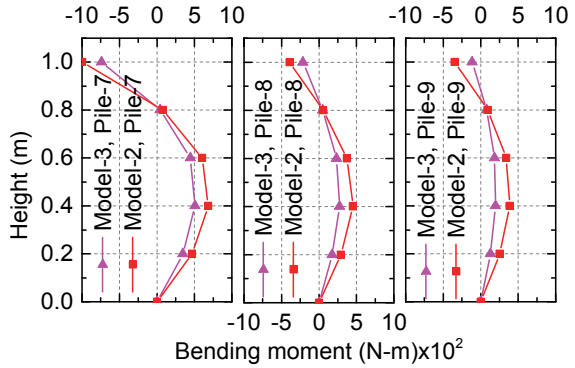

Figure 17: Comparison of the seismic response of piles in Model-2 & Model-3.

7 CONCLUSIONS

This paper describes the seismic response of pile-supported bridge abutment. A fully-coupled 3-D FE analysis is adopted here. A large-scale shake table test of a model abutment designed based on the current Japanese standard is simulated. Another two model abutments designed based on the old Japanese standard with the different geometrical shape of the embankment are also analyzed to observe the strut effect of bridge girder and the influence of the width of the embankment on the failure mechanism of the bridge abutment. The key findings of this study can be summarized as follows;

The 3-D Finite Element Analysis can capture the overall response of the bridge abutment subjected to lateral spreading although the magnitudes of measured parameters for example pore water pressure, horizontal displacement, and bending moment, are different.

Accumulation of displacement of both soil and abutment starts with the generation of excess pore water pressure. Significant permanent displacement of soil and as well as structural system toward the channel may take place if the foundation soil gets liquefied.

The maximum bending moment takes place near the head of the piles in all kinds of arrangement. The development of the maximum bending moment in pile is not necessarily coincided with the arrival of the principal shock. A backward rotation of the abutment is observed due to strut effect of the bridge girder.

Removal of the extended part of the embankment outside of the approach road may reduce the maximum bending moment up to 25%.

ACKNOWLEDGEMENT

The authors would like to acknowledge the contribution of Public Works Research Institute in this study by allowing us to use their experimental results.

REFERENCES

Asaoka, A. et al., 2002. An elasto-plastic description of two distinct volume change mechanisms of soils. *Soils and Foundations*, 42(5), pp.47–57.

Amiri, S.K., 2008. The earthquake response of bridge pile foundations to liquefaction-induced lateral spread displacement demands. Doctoral dissertation, University of Southern California.

Antoniou, S. & Pinho, R., 2016. SeismoSignal.

Bartlett, S.F. & Youd, T.L., 1992. Case histories of lateral spreads caused by the 1964 Alaska earthquake, in Case Studies of Liquefaction and Lifeline Performance During Past Earthquakes: U.S. National Center for Earthquake Engineering Research Technical Report NCEER-92-0002, v. 2.

Japan Road Association, 1964. Design guideline for substructures for highway bridges.

Japan Road Association, 2002. Specifications for highway bridges-Part V seismic design, Tokyo, Japan.

Kramer, S.L., 1996. Geotechnical Earthquake Engineering, Pearson Education India.

Motamed, R. et al., 2013. Pile group response to liquefaction-induced lateral spreading: E-Defense large shake table test. *Soil Dynamics and Earthquake Engineering*, 51, pp.35–46.

Takahashi, A., 2002. Soil – pile interaction in liquefaction-induced lateral spreading of soils. DEng. dissertation, Tokyo Institute of Technology.

Takahashi, A., Sugita, H. & Tanimoto, S., 2010. Forces acting on bridge abutments over liquefied ground. *Soil Dynamics and Earthquake Engineering*, 30(3), pp.146–156.

Muir Wood, D., 2004. Geotechnical modelling, Applied Geotechnics, Vol. 1, Taylor & Francis.

Yoshimi, Y., Keizo, T. & Tokimatsu, K., 1989. Liquefaction resistance of a partially saturated sand. *Soils and Foundations*, 29(3), pp.157–162.